

## Supplemental Information for: Low Temperature CO Oxidation over Rh Supported on N-Doped Carbon

Colby A. Whitcomb,<sup>a</sup> Anukriti Shrestha,<sup>a</sup> Christopher Paolucci,<sup>a\*</sup> and Robert J. Davis<sup>a\*</sup>

\*Corresponding authors

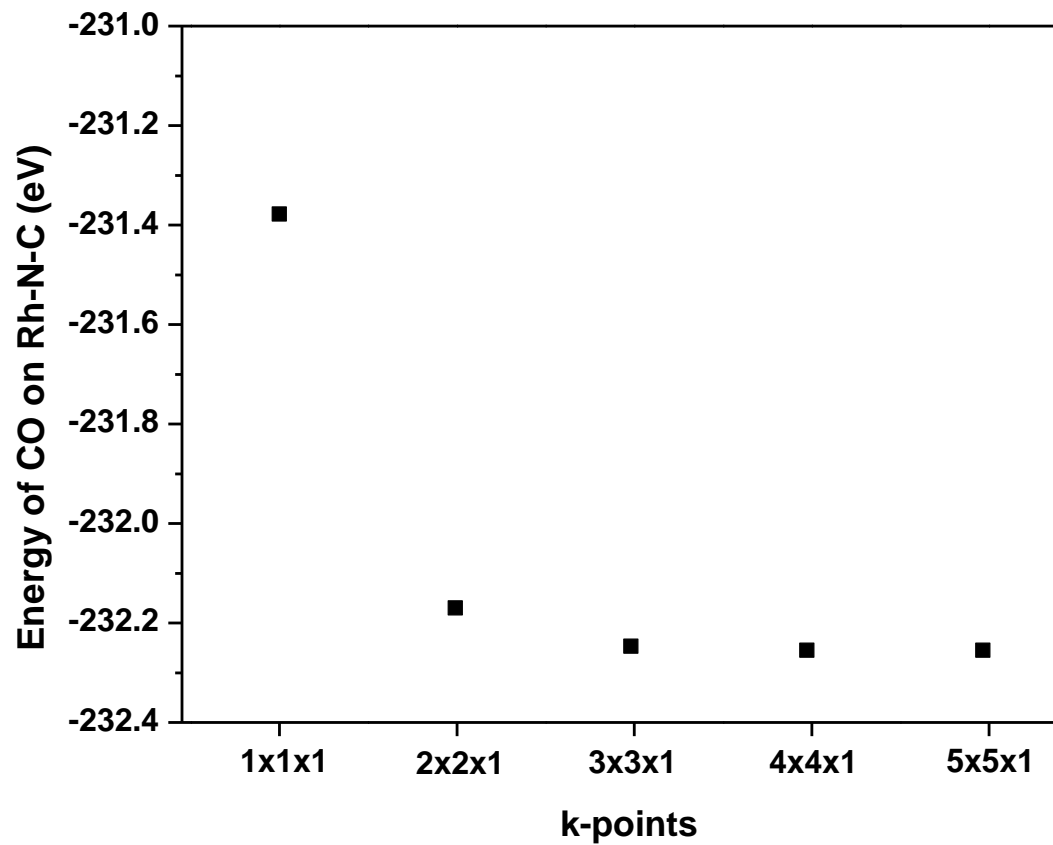
<sup>a</sup>Department of Chemical Engineering, University of Virginia, 351 McCormick Road, Charlottesville, VA 22904

### Supplemental Figures:

<b>Supplemental Fig. S1.</b> Optimization of the Monkhorst Pack k-point mesh for the small cell (higher density of M) using vdW-DF.....	2
<b>Supplemental Fig. S2.</b> Climbing image nudged elastic band calculations for TS1 and TS2.....	4
<b>Supplemental Fig. S3.</b> Coverage of CO plotted as a function of temperature based on theoretical binding energy. ....	5
<b>Supplemental Fig. S4.</b> Coverage of CO and O <sub>2</sub> as a function of the difference in enthalpy of binding energy. ....	6
<b>Supplemental Fig. S5.</b> Energy along the reaction coordinate for the Rh-N-C structure from vdW-DF with either a CO or O <sub>2</sub> adsorbate on the “bottom” of the structure.....	7
<b>Supplemental Fig. S6.</b> a) Magnetic states of the entire structure during calculations of CO and O <sub>2</sub> binding energy. b) Magnetic state of the metal atom in the bare structure or after binding of CO or O <sub>2</sub> . ....	8
<b>Supplemental Fig. S7.</b> Climbing image nudged elastic band calculation for TS1 using the PBE functional. ....	<b>Error! Bookmark not defined.</b>
<b>Supplemental Fig. S8.</b> Density of States for Rh atom along the reaction coordinate in Fig 2. ....	100
<b>Supplemental Fig. S9.</b> Arrhenius-type plots for CO oxidation on various Rh-containing catalysts. ....	111
<b>Supplemental Fig. S10.</b> Reaction order plots for both CO and O <sub>2</sub> on various Rh-containing catalysts during the CO oxidation reaction.....	12

### Supplemental Table:

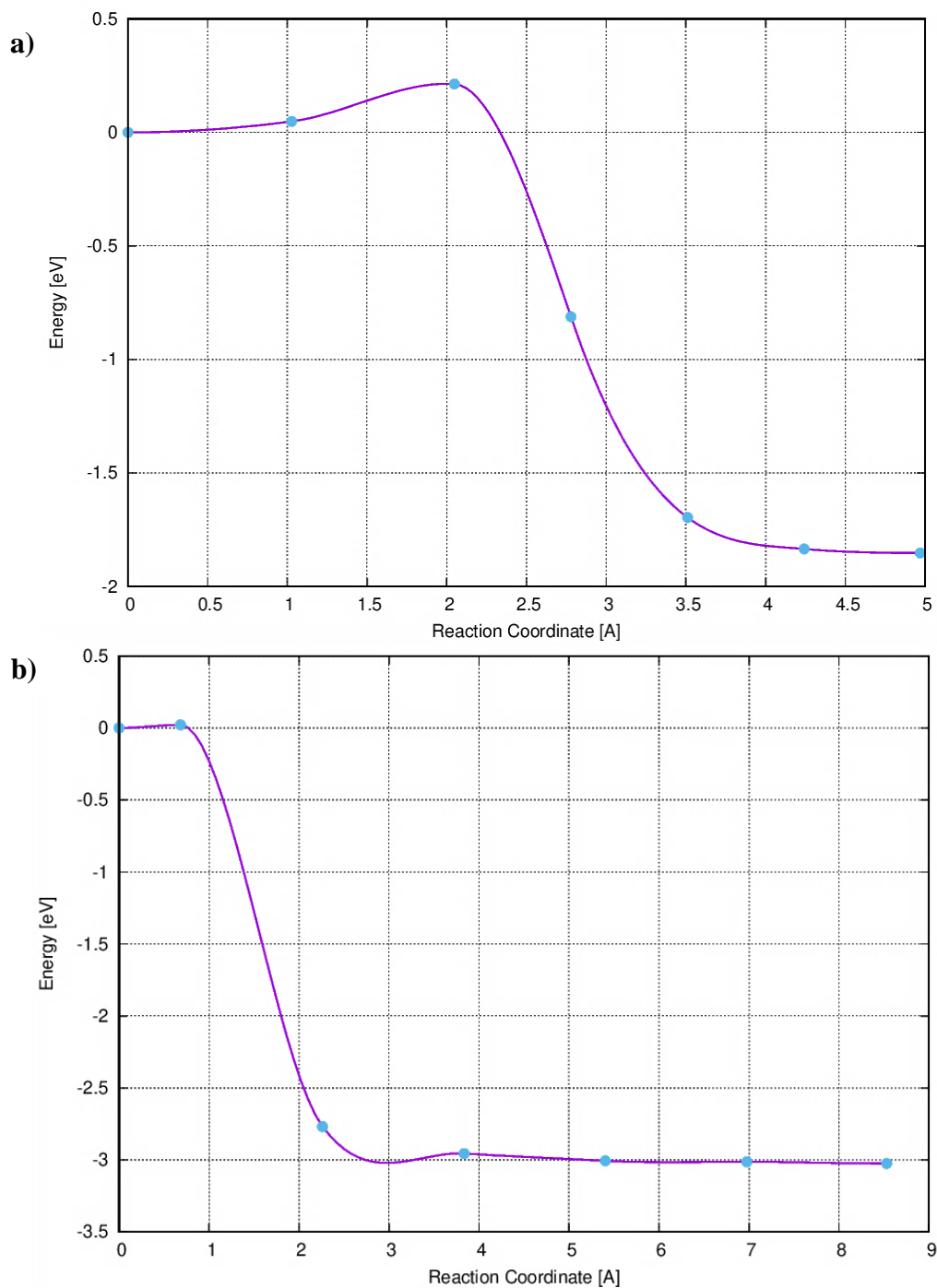
<b>Supplemental Table S1.</b> Comparison of Binding Energy for CO and O <sub>2</sub> from our PBE calculations versus PBE literature values.....	3
<b>Supplemental Table S2.</b> Charge density from Bader charge analysis for Rh atom over the reaction coordinate from Fig. 2.....	9



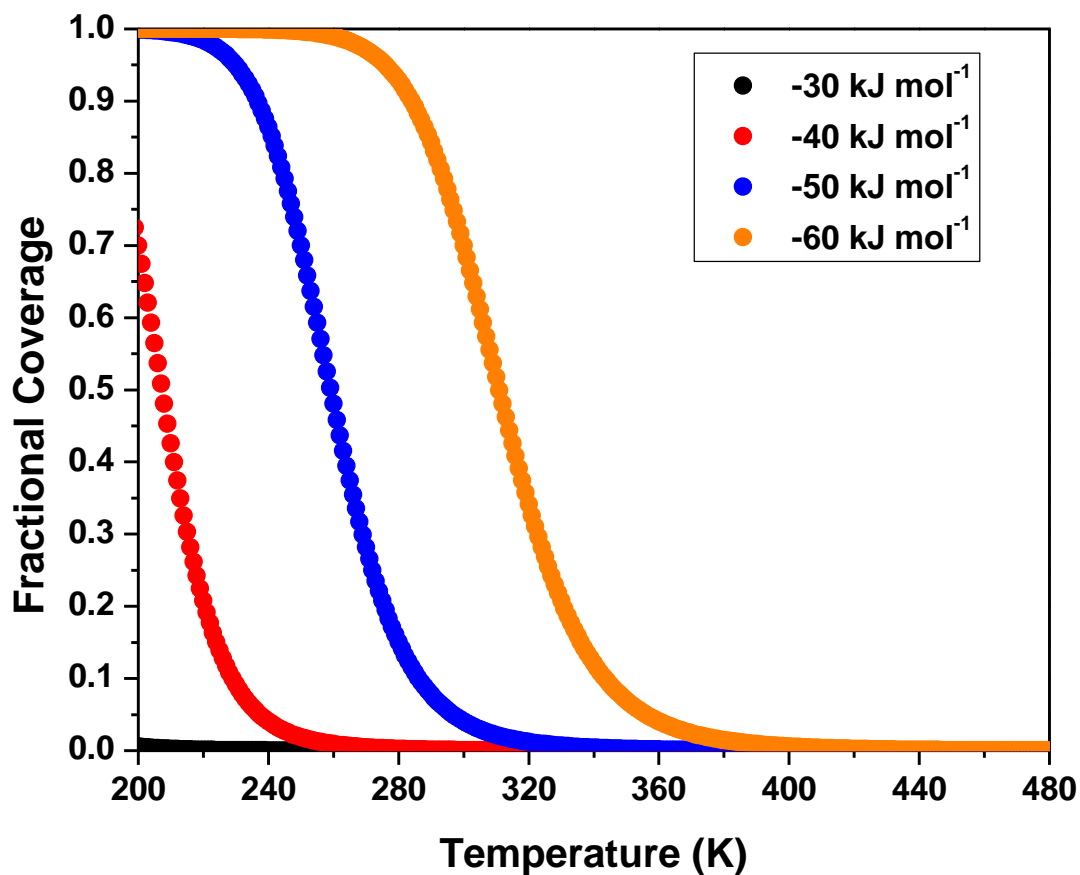
**Supplemental Fig. S1.** Optimization of the Monkhorst Pack k-point mesh for the small cell (higher density of M) using vdW-DF.

**Supplemental Table S1.** Comparison of Binding Energy for CO and O<sub>2</sub> from our PBE calculations versus PBE literature values

Element		Binding Energy	Literature Binding Energy <sup>1</sup>
<b>Ag</b>	BE <sub>CO</sub>	0	0
	BE <sub>O2</sub>	-13	-9
<b>Au</b>	BE <sub>CO</sub>	-1	-1
	BE <sub>O2</sub>	-22	-14
<b>Co</b>	BE <sub>CO</sub>	-73	-77
	BE <sub>O2</sub>	-61	-69
<b>Cr</b>	BE <sub>CO</sub>	-90	-105
	BE <sub>O2</sub>	-182	-198
<b>Cu</b>	BE <sub>CO</sub>	0	-1
	BE <sub>O2</sub>	-8	-10
<b>Fe</b>	BE <sub>CO</sub>	-146	-78
	BE <sub>O2</sub>	-73	-94
<b>Ir</b>	BE <sub>CO</sub>	-104	-114
	BE <sub>O2</sub>	-40	-48
<b>Mn</b>	BE <sub>CO</sub>	-102	-108
	BE <sub>O2</sub>	-124	-130
<b>Ni</b>	BE <sub>CO</sub>	-1	-2
	BE <sub>O2</sub>	-6	-7
<b>Pd</b>	BE <sub>CO</sub>	-1	-1
	BE <sub>O2</sub>	-5	-4
<b>Pt</b>	BE <sub>CO</sub>	-1	-2
	BE <sub>O2</sub>	-4	-4
<b>Rh</b>	BE <sub>CO</sub>	-73	-82
	BE <sub>O2</sub>	-54	-57
<b>Ru</b>	BE <sub>CO</sub>	-262	-260
	BE <sub>O2</sub>	-177	-171

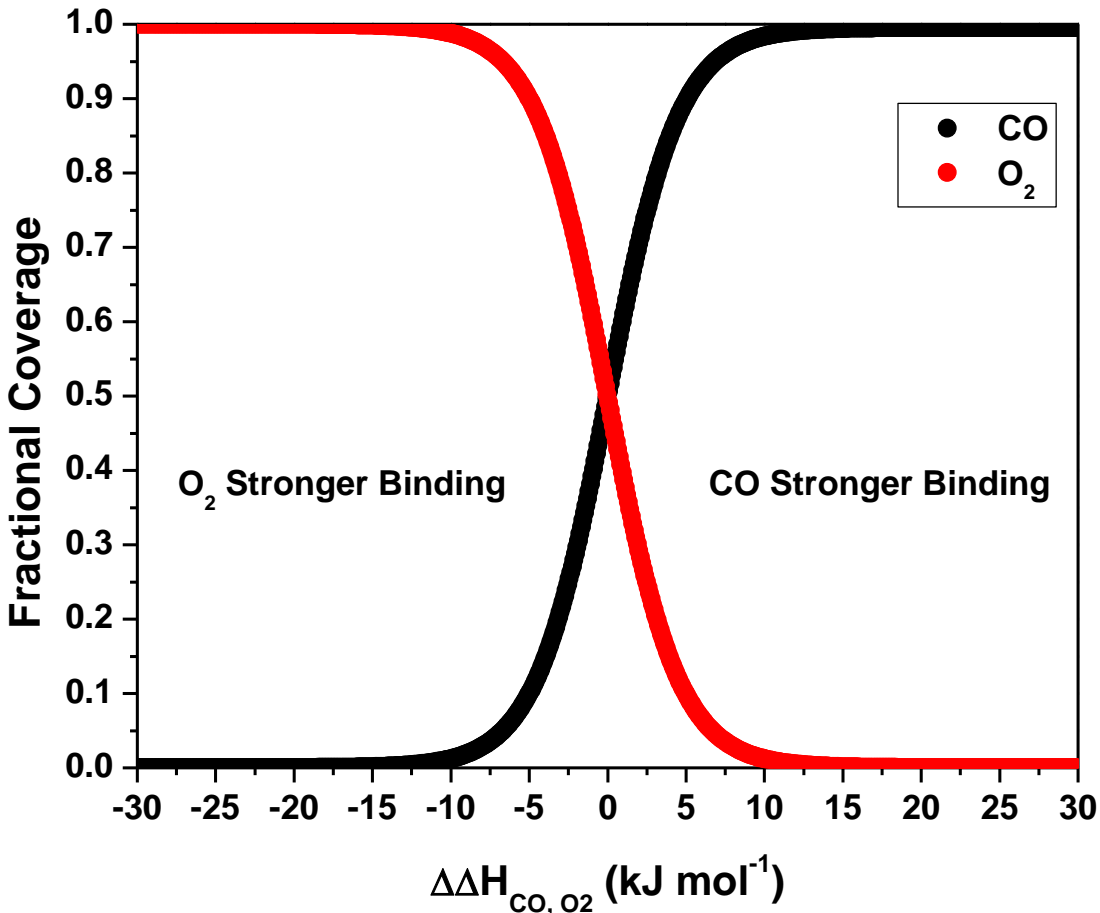


**Supplemental Fig. S2.** Climbing image nudged elastic band calculations for TS1 and TS2. Plots for CI-NEB for TS1 (a) and TS2 (b). a and b were calculated with vdW-DF and NUPDOWN set to 0.



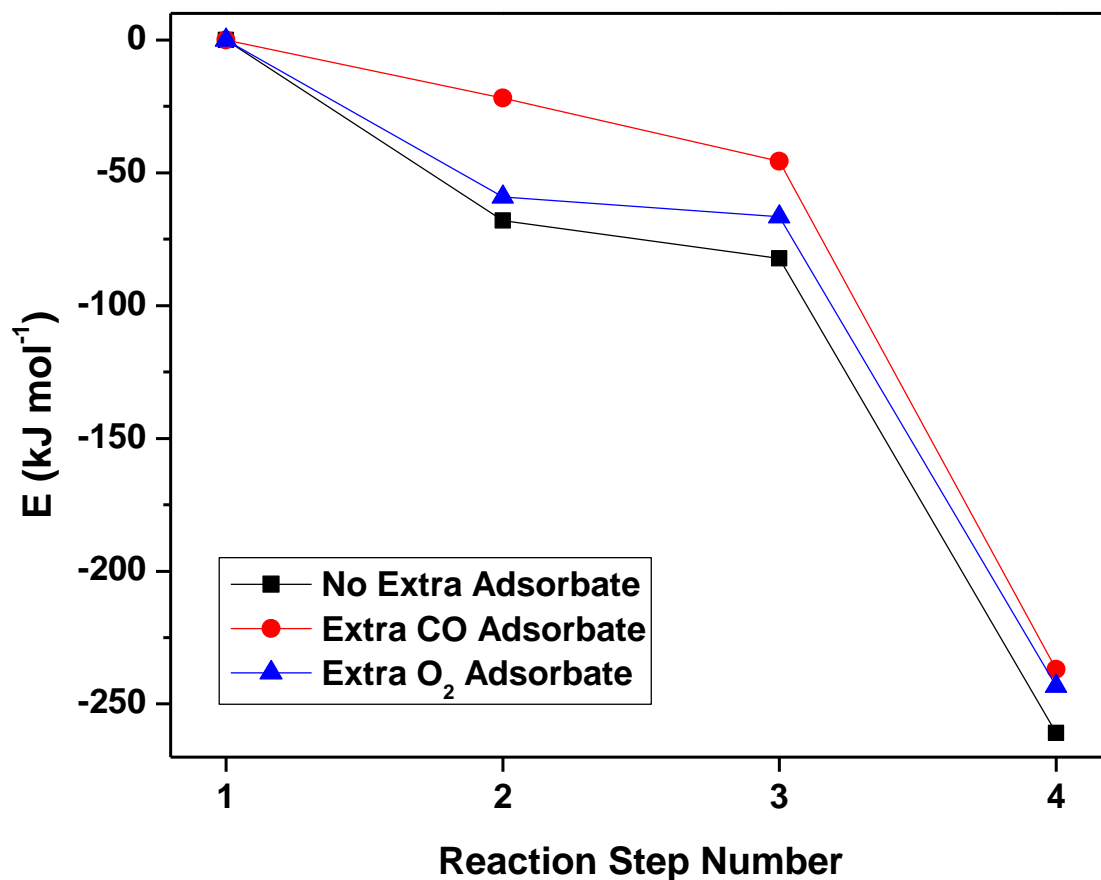
**Supplemental Fig. S3.** Coverage of CO plotted as a function of temperature based on theoretical binding energy.

Pressure was fixed at 1 bar and the standard entropy of adsorption was assumed to be  $-2 \text{ meV K}^{-1}$ .<sup>1,2</sup> Previous reports on variation in the binding energy based on functional choice led us to expand our criterion by  $10 \text{ kJ mol}^{-1}$ , indicating that  $-30 \text{ kJ mol}^{-1}$  is a conservative cutoff for the binding energy of CO.<sup>3</sup> Metals that have a binding energy weaker than  $-30 \text{ kJ mol}^{-1}$  would not result in significant coverage at the temperatures explored in this study.



**Supplemental Fig. S4.** Coverage of CO and O<sub>2</sub> as a function of the difference in enthalpy of binding energy.

The  $\Delta\Delta H_{\text{CO},\text{O}_2}$  term is defined as  $\Delta H_{\text{O}_2} - \Delta H_{\text{CO}}$  where  $\Delta H_{\text{CO}}$  is fixed at  $-67 \text{ kJ mol}^{-1}$  and the binding energy of O<sub>2</sub> is varied. The temperature is set at 273 K with pressures of CO and O<sub>2</sub> each set to 1 bar. The standard entropy of adsorption is assumed to be  $-2 \text{ meV K}^{-1}$ .<sup>2</sup> This analysis suggests binding energies within  $20 \text{ kJ mol}^{-1}$  are necessary for non-negligible CO coverage. Combining this with previous reports for  $\sim 10 \text{ kJ mol}^{-1}$  variation in binding energies based on functional and cell size suggest  $30 \text{ kJ mol}^{-1}$  as a conservative cutoff for the difference in O<sub>2</sub> and CO binding energies.<sup>3</sup> If O<sub>2</sub> is  $30 \text{ kJ mol}^{-1}$  stronger binding to the metal compared to CO then it will result in O<sub>2</sub> completely replacing CO on the metal site at the temperatures in this study.



**Supplemental Fig. S5.** Energy along the reaction coordinate for the Rh-N-C structure from vdW-DF with either a CO or O<sub>2</sub> ligand bonded to Rh on the bottom of the structure.

The reaction coordinate is the same as the one in Figure 2. For example, step one is bare, with a CO ligand initially, or with an O<sub>2</sub> ligand initially. Adding either extra adsorbate resulted in a less exothermic binding of the O<sub>2</sub> to the bound CO.

Since structures that bind CO too weakly would likely bind a second adsorbate even weaker, we investigated the two structures that fit the first two criteria (binds CO and is not outcompeted by O<sub>2</sub>) but did not meet the third criterion, i.e., Fe-N-C and Ru-N-C, to explore the effect of an additional ligand further. The third criterion is the formation of a stable CO-O<sub>2</sub> complex. Upon the addition of the CO or O<sub>2</sub> ligand to the side of the metal opposite the CO-O<sub>2</sub> complex different results were observed. After addition of the O<sub>2</sub> ligand, neither Fe-N-C or Ru-N-C converged to a stable CO-O<sub>2</sub> complex, consistent with the absence of an adsorbate. For CO on Ru-N-C, the adsorption of the second CO to the other side of Ru-N-C is endothermic, precluding this path. For Fe-N-C, addition of the second CO is exothermic and does enable convergence to a local minimum for the CO-O<sub>2</sub> complex, however, its formation is endothermic, which contrasts with Rh-N-C and Co-N-C, and may explain why low temperature (200 K) CO oxidation activity is not experimentally observed on Fe-N-C materials (see ref. 12 in the main text). Thus, although we cannot exhaustively rule out other potential mechanisms for CO oxidation on Fe-N-C and Ru-N-C, our results suggest that the low temperature mechanism explored in this manuscript is not viable on Fe-N-C and Ru-N-C, regardless of the existence of an axial CO/O<sub>2</sub> ligand.

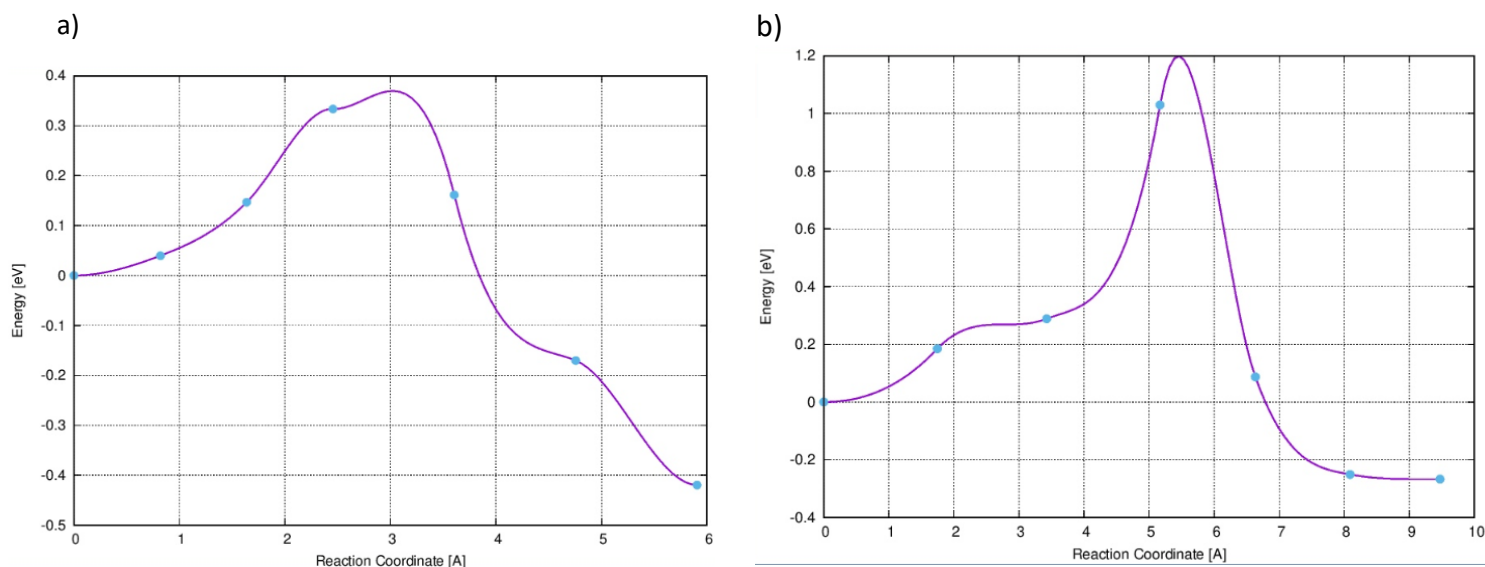
a)

Cr		Mn		Fe		Co		Ni		Cu		Zn		Ga	
CO	2.0	CO	1.1	CO	0.1	CO	0.7	CO	0	CO	1.1	CO	0	CO	0.3
O <sub>2</sub>	2.0	O <sub>2</sub>	3.0	O <sub>2</sub>	1.8	O <sub>2</sub>	1.1	O <sub>2</sub>	1.9	O <sub>2</sub>	2.8	O <sub>2</sub>	1.5	O <sub>2</sub>	1.0
Magnetic States from vdW-DF optimizations				Ru		Rh		Pd				Cd			
				CO	0	CO	0	CO	0			CO	0		
				O <sub>2</sub>	-1.3	O <sub>2</sub>	1.0	O <sub>2</sub>	1.8			O <sub>2</sub>	1.3		
						Ir		Pt		Au					
				CO	0	CO	0	CO	0						
				O <sub>2</sub>	1.0	O <sub>2</sub>	1.8	O <sub>2</sub>	1.7						

b)

Cr		Mn		Fe		Co		Ni		Cu		Zn		Ga	
Bare	3.4	Bare	2.9	Bare	1.9	Bare	0.7	Bare	0	Bare	0.5	Bare	0	Bare	0
CO	1.9	CO	1.2	CO	0	CO	0.5	CO	0	CO	0.5	CO	0	CO	0
O <sub>2</sub>	2.5	O <sub>2</sub>	2.3	O <sub>2</sub>	1.5	O <sub>2</sub>	0.1	O <sub>2</sub>	0	O <sub>2</sub>	0.5	O <sub>2</sub>	0	O <sub>2</sub>	0
Magnetic States of Metal Atoms from vdW-DF optimizations				Ru		Rh		Pd				Cd			
				Bare	1.2	Bare	0.3	Bare	0			Bare	0		
				CO	0	CO	0	CO	0			CO	0		
				O <sub>2</sub>	1.0	O <sub>2</sub>	0	O <sub>2</sub>	0			O <sub>2</sub>	0		
				Ir		Pt		Au							
				Bare	0.4	Bare	0	Bare	0.3						
				CO	0	CO	0	CO	0						
				O <sub>2</sub>	0	O <sub>2</sub>	0	O <sub>2</sub>	0.3						

**Supplemental Fig. S6.** a) Magnetic states of the entire structure during calculations of CO and O<sub>2</sub> binding energy. b) Magnetic state of the metal atom in the bare structure or after binding of CO or O<sub>2</sub>.

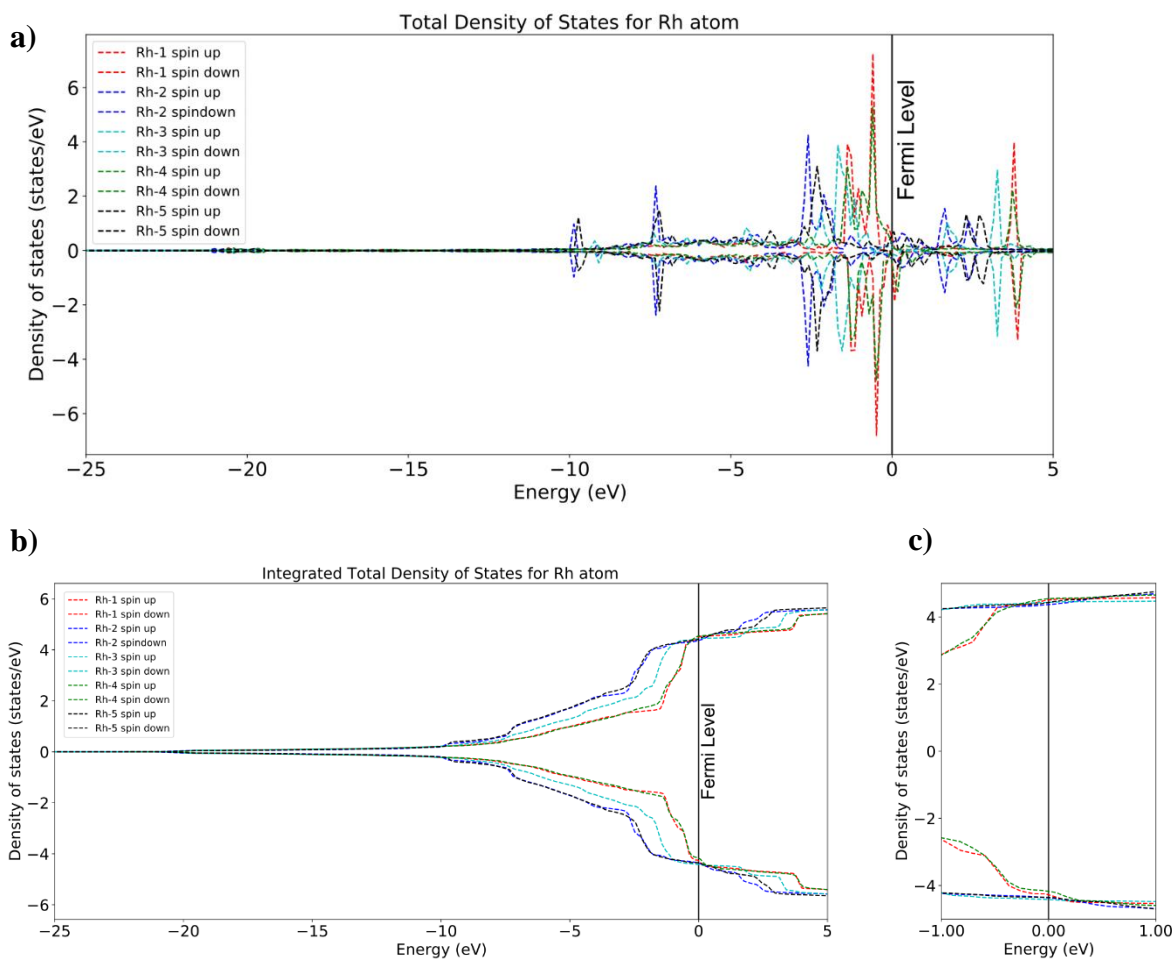


**Supplemental Fig. S7.** Investigation of the mobility of the O atom from step 4 in Fig. 2. a) Nudged elastic band calculation for the migration of the O atom from the carbon to metal site using the vdW-DF functional with 1 metal atom per 0.8 nm<sup>2</sup>. b) Nudged elastic band calculation for the same reaction with a lower Rh density of 1 metal atom per 1.3 nm<sup>2</sup>. The difference in the diffusion barriers in the two cells is a consequence of the reaction coordinate involving significant distortion of the graphene plane.

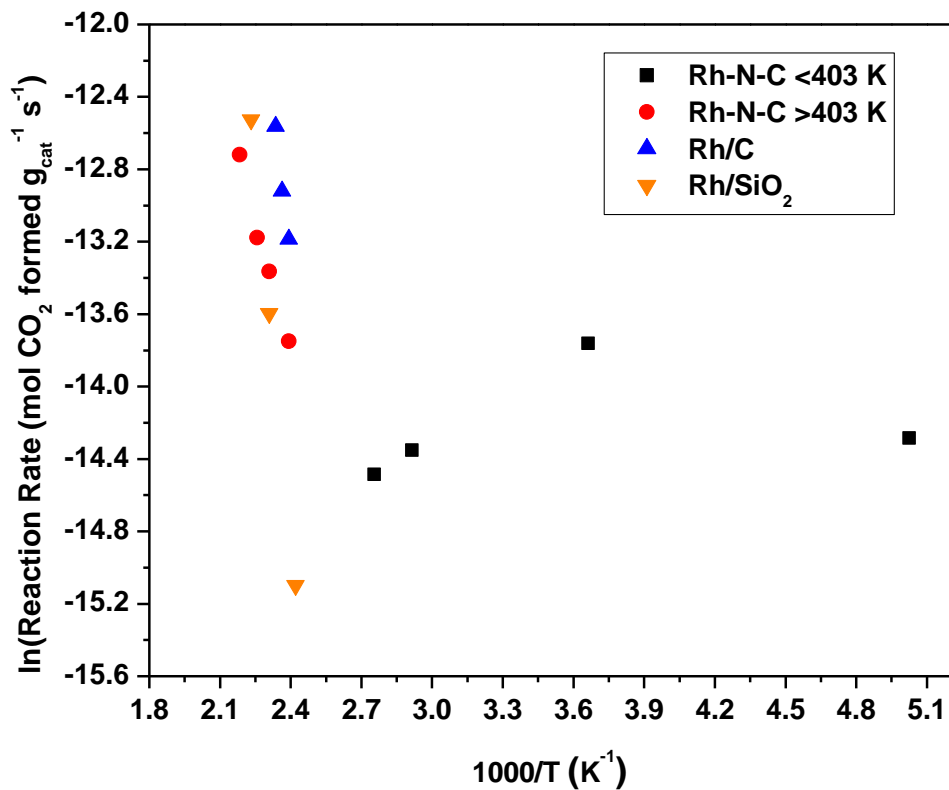
**Supplemental Table S2.** Charge density from Bader charge analysis for Rh atom over the reaction coordinate from Fig. 2.

The Bader charges were computed using the method developed by Henkelman et al.<sup>4,5</sup>

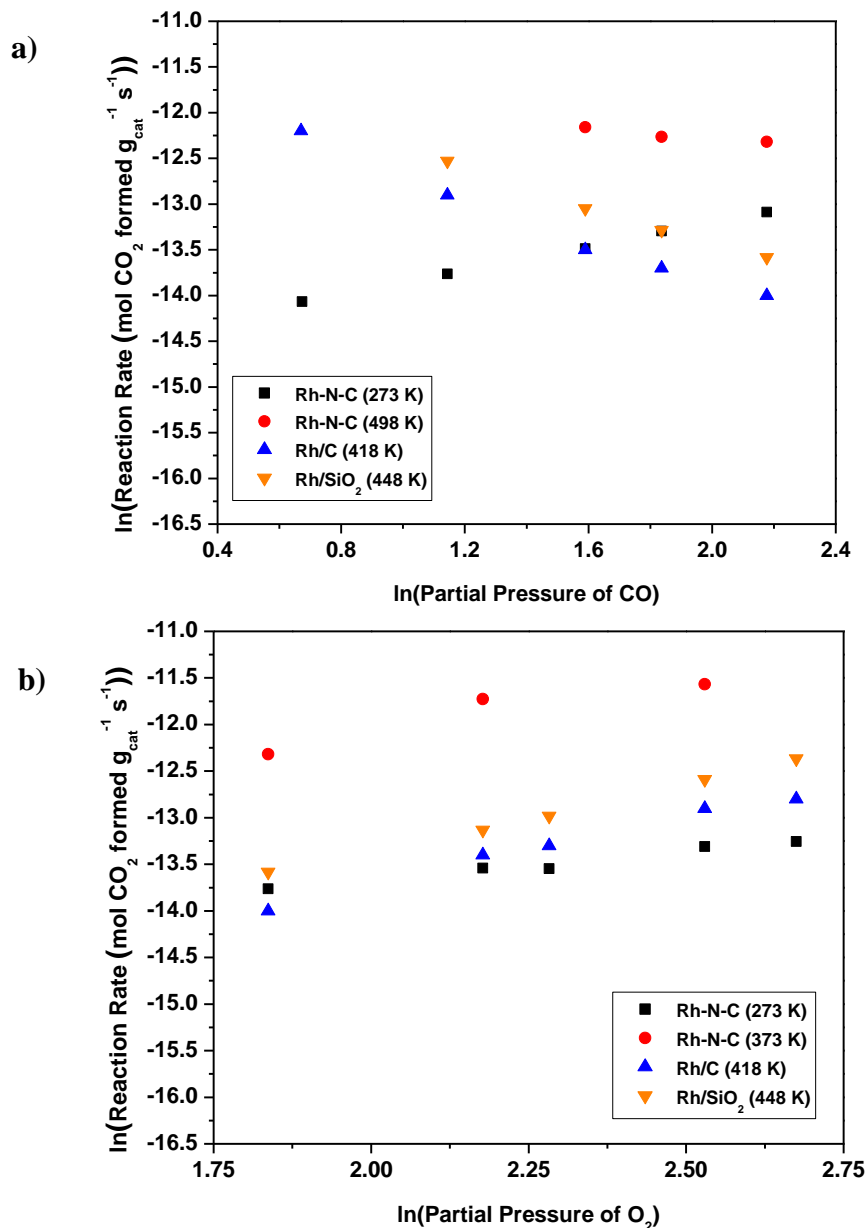
Reaction Coordinate	Charge
1	8.0
2	7.8
3	7.8
4	8.0
5	7.7



**Supplemental Fig. S7.** Density of States for Rh atom along the reaction coordinate in Fig 2. a) The total density of states for the Rh atom. b) the integrated density of states for Rh atom. c) inset of panel b showing a close-up image of the Fermi level. The numbers in the legend for the figures correspond to the reaction coordinate in Fig. 2.



**Supplemental Fig. S8.** Arrhenius-type plots for CO oxidation on various Rh-containing catalysts. The reaction was run with 0.2 g of catalyst diluted in SiC and with 160 cm<sup>3</sup> total flow, 1 % CO, 2 % O<sub>2</sub>, and balance He at 3 atm. The O<sub>2</sub> and CO were purified with silica traps in a dry-ice acetone bath while the He was purified with an OMI filter. All of the points were collected at steady-state and were collected by alternating between low and high temperature.



**Supplemental Fig. S9.** Reaction order plots for both CO and O<sub>2</sub> on various Rh-containing catalysts during the CO oxidation reaction.

- Plot of the effect of the partial pressure of CO on the reaction rate for various Rh-containing catalysts by varying the partial pressure (2.0 to 8.8 kPa) of CO and holding the O<sub>2</sub> constant at 6.3 kPa
- Plot of the effect of the partial pressure of O<sub>2</sub> on the reaction rate for various Rh-containing catalysts by varying the partial pressure (6.3 to 14.5 kPa) of O<sub>2</sub> and holding the CO constant at 8.8 kPa for all catalysts except the Rh-N-C which collected at 3.1 kPa. The temperatures were adjusted to give < 15 % conversion. It was difficult to maintain low conversion for the highest partial pressures of both CO and O<sub>2</sub> for the Rh-N-C (373 K) sample, but the conversion was < 30 %.

## References

1. T. Kropp and M. Mavrikakis, *ACS Catal.*, 2019, **9**, 6864-6868.
2. J. K. Nørskov, F. Studt, F. Abild-Pedersen and T. Bligaard, *Fundamentals of Heterogeneous Catalysis*, John Wiley & Sons, 2014.
3. C. A. Whitcomb, A. Sviripa, M. I. Schapowal, K. Mamedov, R. R. Unocic, C. Paolucci and R. J. Davis, *ACS Catal.*, 2022, **12**, 15529-15540.
4. W. Tang, E. Sanville and G. Henkelman, *J. Phys.: Condens. Matter.* 2009, **21**, 084204.
5. E. Sanville, S. D. Kenny, R. Smith and G. Henkelman, *J. Comput. Chem.* 2007, **28**, 899-908.